

Towards Cross-device and Training-free Robotic Grasping in 3D Open World

Weiguang Zhao^{1*}, Chenru Jiang^{2*}, Chengrui Zhang³, Jie Sun⁴, Yuyao Yan⁵, Rui Zhang^{6†}, Kaizhu Huang⁷

Abstract— **Robotic grasping in the open world** is a critical component of manufacturing and automation processes. While numerous existing approaches depend on 2D segmentation output to facilitate the grasping procedure, accurately determining depth from 2D imagery remains a challenge, often leading to limited performance in complex stacking scenarios. In contrast, techniques utilizing 3D point cloud data inherently capture depth information, thus enabling adeptly navigating and manipulating a diverse range of complex stacking scenes. However, such efforts are considerably hindered by the variance in data capture devices and the unstructured nature of the data, which limits their generalizability. Consequently, much research is narrowly concentrated on managing designated objects within specific settings, which confines their real-world applicability. This paper presents a novel pipeline capable of executing object grasping tasks in open-world scenarios even on previously unseen objects without the necessity for training. Additionally, our pipeline supports the flexible use of different 3D point cloud segmentation models across a variety of scenes. Leveraging the segmentation results, we propose to engage a training-free binary clustering algorithm that not only improves segmentation precision but also possesses the capability to cluster and localize unseen objects for executing grasping operations. In our experiments, we investigate a range of open-world scenarios, and the outcomes underscore the remarkable robustness and generalizability of our pipeline, consistent across various environments, robots, cameras, and objects. The code will be made available upon acceptance of the paper.

I. INTRODUCTION

Robotic grasping plays a crucial role in various manufacturing and automation applications [1], [2], [3], [4], [5], [6]. This task typically begins with segmenting the scene and estimating the objects' poses. Once the grasping position is determined, the robot executes the grasping operation. With the rapid advancement of artificial intelligence, the focus of robotic grasping research has gradually shifted from fixed

*Equal contribution

†Corresponding author

¹Weiguang Zhao is with Department of Computer Science, University of Liverpool, L69 7ZX Liverpool, UK weiguang@liverpool.ac.uk

²Chenru Jiang with Data Science Research Center, Duke Kunshan University, Suzhou, 215316, China cj262@duke.edu

³Chengrui Zhang with Department of Electrical Engineering, University of Liverpool, L69 7ZX Liverpool, UK aruix@liverpool.ac.uk

⁴Jie Sun with Department of Mechatronics and Robotics, Xi'an-Jiaotong Liverpool University, Suzhou, 215123, China Jie.Sun@xjtlu.edu.cn

⁵Yuyao Yan with School of Robotic, Xi'an Jiaotong-Liverpool University, Suzhou, 215123, China Yuyao.Yan@xjtlu.edu.cn

⁶Rui Zhang with Department of Foundational Mathematics, Xi'an Jiaotong-Liverpool University, Suzhou, 215123, China Rui.Zhang02@xjtlu.edu.cn

⁷Kaizhu Huang with Data Science Research Center, Duke Kunshan University, Suzhou, 215316, China kaizhu.huang@dukekunshan.edu.cn

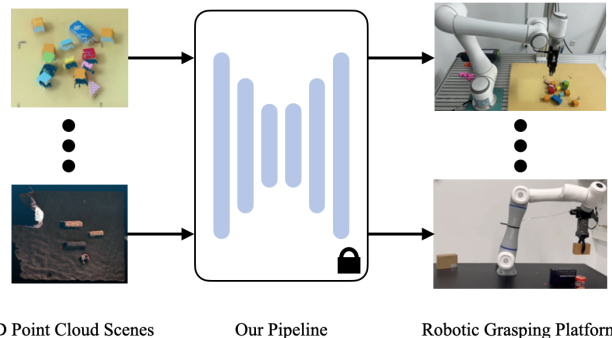


Fig. 1: Illustration of the robotic grasping process in open-world scenarios. The left column displays input point cloud scenes, captured using point cloud acquisition devices of varying precision and types. The right column shows the actual grasping scenes, where two different robots perform object grasping tasks under various scenes. The middle column represents our pipeline, which not only segments and estimates poses in a training-free manner based on different precision point cloud inputs, but also enables different robots to accurately grasp various unseen objects.

environments to more challenging open-world scenarios. Traditional segmentation and pose estimation methods [7], [8] often struggle with complex scenes involving stacked or occluded objects. Current methods based on Convolutional Neural Networks (CNNs) typically process RGB [9], [10], [11] or RGB-D [12], [13], [14], [15] data. While these methods still focus on extracting texture features from 2D image information for predictions, they face limitations when handling textureless objects, poor lighting conditions, or cluttered environments. Fortunately, researchers have found that incorporating rich depth information can effectively address these challenges. In particular, point clouds, with inherent depth information, simple structure, and low computational requirements, have gained widespread attention in the research community.

3D point cloud data provides rich geometric information, such as surface point coordinates and normals. Since depth data is directly measured, point clouds offer clear advantages when handling textureless objects, poor lighting conditions, and complex scenes. Currently, mainstream robotic grasping methods based on 3D point cloud data can be divided into two categories: 1) methods that train networks for specific scenarios [16], [17], [18], and 2) training-free methods based on clustering algorithms [19], [20], [21]. Due to the inherent sparsity and irregularity of point cloud data [22], [23], the former relies on training customized networks for a fixed number of points and specific scenarios. Therefore, the generalization of such methods is significantly limited

by variations in point cloud data caused by cross-device or cross-scenario differences. The latter, albeit training-free, still faces challenges such as incorrect object center estimation due to the data loss, and difficulty in separating adjacent objects due to the distance-based clustering. As a result, a significant gap remains for these models to be applied in practical scenarios. In response to these challenges, we propose a novel pipeline that is both cross-device and training-free, enabling our method to be easily deployed for robotic grasping tasks in open-world scenarios.

The advantage of our pipeline lies in its superior generalization ability, enabling it to adapt across devices with varying hardware precision in open-world scenarios. Additionally, thanks to our binary clustering with point density, it delivers reliable grasping performance for both seen and unseen objects without any training. A simple process demonstration of our pipeline is shown in Fig. 1.

In terms of generalization, our pipeline does not rely entirely on CNN results for scene segmentation, which enables superior generalization across different devices. Specifically, we adopt CNNs only for simple foreground and background segmentation of 3D point cloud scenes, followed by our training-free clustering method for accurate object segmentation. This approach minimizes the impact of inaccuracies in object segmentation caused by CNNs when deployed on different devices. Consequently, our pipeline can be deployed on hardware with significant precision differences to handle various complex open-world scenarios. For instance, in our experiments, the two depth cameras used differ by nearly one million in the number of point clouds.

In terms of the clustering algorithm, our developed binary clustering leverages the entirety of point data to accurately determine object centers. Furthermore, our algorithm performs clustering based on point density, which is advantageous for segmenting adjacent objects, thereby ensuring accurate segmentation. This binary clustering algorithm can be readily integrated with various segmentation models to further improve segmentation accuracy and can cluster and locate unseen objects, enabling different segmentation models to demonstrate efficient and reliable performance across diverse open-world scenarios.

To validate the robustness and generalization of our model, we conduct a series of experiments, creating several complex scenes and deploying various robots and cameras to grasp arbitrary objects. Moreover, we also test our point cloud segmentation network in our pipeline: our network also demonstrates superior segmentation performance. Overall, the experimental results indicate that our method excels in open-world scenarios and across different hardware devices, even when handling occluded and stacked unseen objects.

The main contributions of our work can be summarized in three folds:

- Our work introduces a novel cross-device and training-free pipeline that can be rapidly deployed on different devices in open-world scenarios, enabling the efficient and reliable grasping of both seen and unseen objects.
- The binary clustering algorithm in our model facilitates

training-free clustering and localization of various unseen objects. It can be integrated into different 3D point cloud segmentation networks without requiring training, further enhancing segmentation accuracy results.

- We design a series of open-world scenarios and apply our pipeline on different robots, conducting grasping experiments in complex scenes using different cameras with varying precision. Experimental results show that our model not only demonstrates satisfactory generalization across different devices, but also exhibits superior robustness in grasping tasks involving complex, unseen objects with occlusions and stacking.

II. RELATED WORK

A. Cross-Device Compatibility

One major challenge in the practical application of robotic grasping is to ensure the generalization of algorithms across different hardware devices, given that hardware often varies in precision. This disparity in precision often leads to sub-optimal model performance when applied to different devices [24]. For example, [16] introduced a large-scale dataset designed to enhance cross-device compatibility. Sim2Real research [25], [26] focuses on transferring model capabilities from simulated environments to real-world settings. However, this process often requires retraining or domain adaptation to address the differences between simulated and real-world scenes, which limits the generalization of these models across different hardware setups [27]. In contrast, our pipeline can adapt to various hardware devices and effectively addresses a wide range of open-world scenarios.

B. Open-World Grasping

The grasping task has always been a critical challenge in the field of robotics, and grasping in open-world scenarios holds significant value in practical applications. Traditional approaches typically operate this task in a highly controlled way, focusing on specific or predefined objects [28], [29]. They typically suffer from poor generalization in open-world scenarios [24]. With the development of deep learning, researchers have begun to design various CNN networks to handle grasping tasks in open-world scenarios. A network was proposed in [30], [31] for predicting robotic grasp detection and semantic segmentation from RGB images. Similarly, [32], [33] trained a neural network for grasping detection using RGB-D data, demonstrating that multi-modal input can enhance performance. However, these methods have not considered the generalization issue in practical applications. Later, Dex-Net [34] employed large-scale datasets during the network training in order to improve model generalization for grasping a wide variety of objects. This work is still limited as it requires the pre-trained model and the number of object classes. Some other approaches have attempted to address these limitations by e.g. incorporating real-time perception and/or reinforcement learning [18]; this however introduces additional computational cost. In contrast, we propose a novel pipeline, which simply applies the clustering

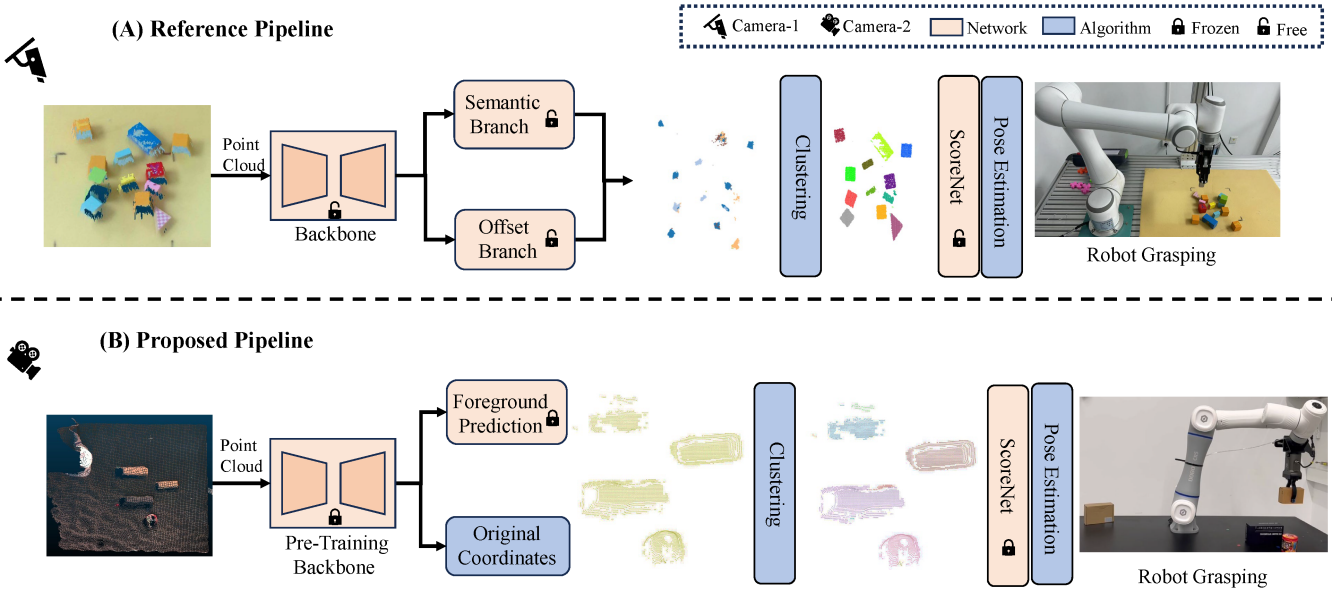


Fig. 2: Overview of proposed method. Reference pipeline stands for the standard robot grasping process leveraging the current 3D segmentation detection method [21], [19], while the proposed pipeline implies the migration of reference pipeline to the robot grasping approach across devices without additional training.

algorithm to handle unseen objects grasping in various open-world scenarios.

C. Training-Free Approaches

With the emergence of Large Language Models (LLM) and Vision-Language Models (VLM), the focus of robotic grasping research has gradually shifted to training-free approaches, with many recent 2D-based studies integrating these models into their works [35], [36]. However, most VLM methods are not particularly effective for handling complex 3D scenes due to object occlusions. Other multi-modality VLM methods [37], [38] still require fine-tuning the model on specific 3D data. Furthermore, the VLM is ineffective for processing 3D point cloud due to the intrinsic irregularity and sparsity of 3D data [22], [23]. Consequently, clustering algorithms, based on 3D point cloud input, gained considerable attraction to achieve training-free robotic grasping [20], [39], [40]. Unfortunately, occluded objects cannot be effectively separated in current works due to the reliance on distance-based clustering. In contrast, our proposed pipeline utilizes a density-based approach to cluster objects in a way that is both effective and distinguishable.

III. PROPOSED METHOD

A. Overview

As shown in Fig. 2, we offer a universal 3D open-world robot grasping pipeline across devices (cameras & robots), which leverages the pre-training model of reference pipeline to detect and score objects directly. Specifically, our proposed pipeline includes mainly: 1) Data collection, 2) Point cloud feature processing, 3) Object clustering, and 4) Robot grasping. First, we feed the point cloud data (xyz) into the backbone network to achieve the point cloud feature. Moreover, we optimize the semantic branch from the reference pipeline to obtain the foreground prediction

and remove the background points. Furthermore, we develop the binary clustering [19] to get the object instance and utilize the ScoreNet to assign scores to each instance, thus determining the grasping order for the robot. Finally, the object segmentation results serve as the basis for the robot's grasping posture. More details of the methods are presented in the following sub-sections.

B. Data Collection

Our method is based on the eye-to-hand approach, with a camera fixed in a suspended position above the grasping scene. At the outset, we extract a frame of video data and convert it into point cloud format, comprising coordinate data $xyz \in \mathbb{R}^{N \times 3}$, texture data $rgb \in \mathbb{R}^{N \times 3}$, and normal data $nl \in \mathbb{R}^{N \times 3}$, where N stands for the number of points. Note that the coordinate data is a must, while texture and normal data are both optional. Moreover, the camera position and brand can be changed, and after any changes, hand-eye calibration is performed to establish the relationship between the camera coordinate system and the robot coordinate system. In this paper, we transform the camera coordinate system to the robot coordinate system, and through hand-eye calibration, we could obtain the corresponding rotation matrix $R \in \mathbb{R}^{3 \times 3}$ and translation matrix $T \in \mathbb{R}^{3 \times 3}$.

C. Point Cloud Feature Processing

Following existing 3D segmentation and detection works [21], [41], [42], [19], the reference pipeline converts the point cloud into a voxel format and utilizes MinkUNet [43] for sparse convolution [44] to obtain voxel features. Subsequently, it converts the voxels back into a point cloud to obtain features. In addition, two branches consisting of MLP layers are leveraged to predict the semantic scores $S \in [0, 1]^{N \times M}$ and the offset $o_i = \{o_x^i, o_y^i, o_z^i\}$ from the

center of the object for each point, where N and M are the number of point and class, where $i \in \{1, \dots, N\}$.

Since the reference pipeline is trained on a dataset containing specific category objects, its semantic branch cannot be applied for open-world object segmentation. For the sake of simplicity, we categorize scenarios into two classes: foreground and background. The foreground includes the objects to be grasped, while the background refers to items such as the tabletop that do not require analytical manipulation. In this regard, we can attain the binary classification score S_b for the foreground and background. The binary classification score $\mathbf{S}_b \in [0, 1]^{N \times 2}$ can be calculated by the semantic score $\mathbf{S} \in [0, 1]^{N \times M}$, from the semantic branch by the following:

$$\mathbf{S}_b^i = [\mathbf{S}^i[1], \max(\mathbf{S}^i[2 : M])] \quad i \in [1, N], \quad (1)$$

where \mathbf{S}_b^i and \mathbf{S}^i represent the binary classification score and semantic classification score for the i_{th} point, respectively. Additionally, $\max(\cdot)$ means the maxpooling operation and $2 : M$ stands the data collection from 2_{th} to M_{th} index. Furthermore, the binary classification prediction $\mathbf{P}_b \in \{0, 1\}$ can be obtained by the following formula:

$$\mathbf{P}_b^i = \text{argmax}(\mathbf{S}_b^i) \quad i \in [1, N], \quad (2)$$

where \mathbf{P}_b^i means the binary classification prediction for i_{th} point. Moreover, $\text{argmax}(\cdot)$ stands for the operation of taking the index of the maximum value. $\mathbf{P}_b^i = 0$ implies i_{th} point is the background point; otherwise, it is the foreground point.

D. Object Detection

The clustering algorithm does not contain network parameters, enabling it to robustly adapt to cross-device 3D object detection. To our best knowledge, PBNet [19] is the best clustering-based 3D instance segmentation method, as recorded in Tab. I. Its binary clustering is employed to attain the preliminary instances, which combine the semantic prediction and the density of each point to group points in the offset coordinate system. Considering that cross-device variations can lead to changes in point cloud features, and thus result in inaccurate predictions of point offset coordinates, we directly cluster the foreground points in the original coordinate system. The detailed clustering steps could be found in Alg. 1.

Furthermore, the MinkUnet [43] serves as the scoring network for assigning scores to each instance. The score for each instance represents the confidence of the instance segmentation, with higher scores indicating better instance segmentation. By analyzing the coordinates of each instance, the bounding box for each target can be computed. The center point coordinate $C \in \mathbb{R}^{N_{ins} \times 3}$ of each object could be achieved by the following formula:

$$C_i = \frac{1}{N_{\text{map}(i)}^I} \sum_{j \in I_{\text{map}(i)}} p_j, \quad (3)$$

where $p_i = \{p_x^i, p_y^i, p_z^i\}$ describes the 3D coordinate of point i in the original point cloud. Moreover, $N_{\text{map}(i)}^I$ is the number of points in prediction instance $I_{\text{map}(i)}$, and N_{ins} stands for the number of the predicted instances.

E. Robot Grasping

The key to adopting 3D segmentation results for robotic object grasping lies in two aspects: the center point of the grasp and the grasp's posture. The center point $Cr \in \mathbb{R}^{N_{ins} \times 3}$ of the grasp could be obtain by the instance center $C \in \mathbb{R}^{N_{ins} \times 3}$:

$$Cr = C \cdot R + T, \quad (4)$$

where R and T are the rotation matrix and translation matrix respectively, obtained from the hand-eye calibration operation. In addition, we suspend the robot's hand above the target object and calculate the yaw angle θ to grasp the target object. θ could be calculated by the point cloud coordinates:

$$\theta = \arctan\left(\frac{y_{xmax} - y_{min}}{x_{ymax} - x_{min}}\right), \quad (5)$$

where y_{min} and x_{min} represents the minimum value of x and y coordinates in the point cloud. Additionally, y_{xmax} denotes the value of y , when x achieves the maximum. Similarly, x_{ymax} stands for the value of x , when y attains the maximum. In our future work, we will consider the open pose of the object and analyze the grasping pose from multiple perspectives.

F. Pseudo-code

For a clearer understanding, we provide the pseudo-code of our cross-device robotic grasping pipeline in Alg. 1.

Algorithm 1: Cross-device robotic grasping

Data: Object confidence threshold: C_θ
 Point Density threshold: d_θ

- 1: **while** True **do**
- 2: Input the newest 3D point cloud scene
- 3: Obtain the foreground point F_p , according to the Eq. 1 and Eq. 2
- 4: Create the point set H_{set} and L_{set}
- 5: **if** The density of $F_p^i > d_\theta$ **then**
- 6: $H_{set}.\text{push_back}(F_p^i)$
- 7: **else**
- 8: $L_{set}.\text{push_back}(F_p^i)$
- 9: **end if**
- 10: Obtain the initial instances I by $\text{Group}(H_{set})$
- 11: Refine the instances I by $\text{Voting}(L_{set})$
- 12: Attain the confidence scores SC of instances I by $\text{ScoreNet}(I)$
- 13: **if** $\max(SC) < C_\theta$ **then**
- 14: break
- 15: **end if**
- 16: Confirm the highest confidence instance I_{idx} by $idx = \text{argmax}(SC)$
- 17: Grasp instance I_{idx} by Eq. 4 and Eq. 5
- 18: **end while**

IV. EXPERIMENTS

For the training-free scene segmentation method comparison, we evaluate our binary clustering across multiple public datasets. For the robotic grasping performance evaluation, we design various open-world scenarios to comprehensively

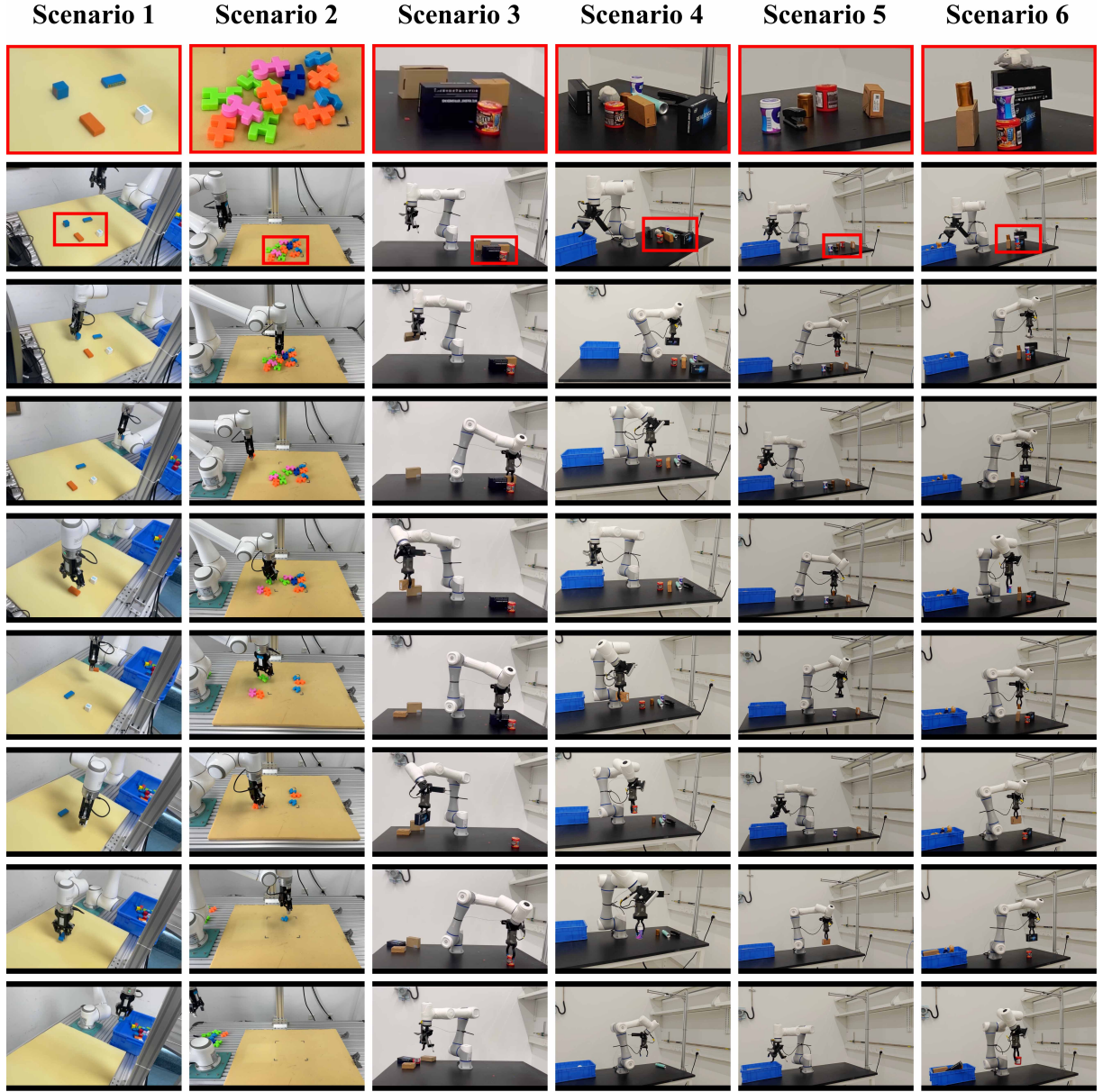


Fig. 3: Illustration of the grasping process in six different open-world scenes with various hardware combinations (robots and cameras). Each column represents a single scene, with the first image being an enlarged view of the scene. The first two columns show the grasping process with hardware combination 1, while the last four columns show the grasping process with hardware combination 2.

assess the proposed pipeline. In each scenario, we test different object distributions, including scattered or clustered arrangements, occluded or stacked placements, and variations in background color. We apply different hardware devices for the experiments, conducting tests with robots from different brands (Elite and Dobot) and cameras (AiNSTEC PRO_L_200_5W: 1624×1240 Depth acc. 0.1% and Intel RealSense D455: 1280×720 Depth acc. 2%).

A. Clustering-based Methods Comparison

We revisit 3D instance segmentation or detection methods based on clustering to seek the best performance of our training-free pipeline. The distance clustering in PointGroup [21] is probably the most popular method, which has been adopted in HAIS [45], MaskGroup [46], and

SoftGroup [20]. On the other hand, the binary clustering in PBNet [19] exhibits the highest performance on the public ScanNetv2 dataset, as recorded in Tab. I. To this end, we incorporate these two clustering methods into our reference pipeline to evaluate their performance in robot grasping on the Boxes dataset, respectively.

Specifically, PointGroup-R represents the integration of PointGroup into our reference pipeline, while PBNet-R signifies the integration of PBNet into our reference pipeline. We report the mean average precision AP (mAP) at overlap 0.25 (AP_{25}), overlap 0.5 (AP_{50}), and overlaps in the range $[0.5:0.95:0.05]$ (AP) for PointGroup-R and PBNet-R in Tab. I. Obviously, PBNet-R is better than PointGroup-R on these three metrics with a performance gain of 27.4%, 12.0%, and 8.0% respectively. Moreover, qualitatively, PBNet-R

also outperforms PointGroup-R, particularly in the stacked scenes as shown in Fig. 4. Building upon these observations, we choose to optimize PBNet for our cross-device robot grasping, as described in the methodology section.

TABLE I: Clustering-based methods compared on 3D point cloud datasets

Datasets	Methods	<i>mAP</i>	<i>AP₅₀</i>	<i>AP₂₅</i>
ScanNetv2 [47]	PointGroup [21]	34.8	56.9	71.3
	SSTNet [48]	40.6	61.0	-
	HAIS [45]	43.5	64.1	75.6
	MaskGroup [46]	42.0	63.3	74.2
	SoftGroup [20]	46.0	67.7	78.9
	RPGN [39]	-	64.2	-
	PBNet [19]	54.3	70.5	78.9
Boxes	PointGroup-R	51.6	84.0	88.0
	PBNet-R	79.0	96.0	96.0

Fig. 4: Segmentation comparison on boxes dataset. Pred. stands for Prediction.

B. Robotic Grasping Comparison

In this section, we construct six real-world scenes to closely simulate open-world object placements. We combine different brands of point cloud acquisition cameras and robots, and then respectively conduct experiments in these six scenarios. The combination 1 is Elite + AiN-STECK PRO_M_200_5W and the combination 2 is Dobot + Intel RealSense D455. During the experiments, the point cloud segmentation network is used solely to separate the foreground and background of the scenes, while subsequent object segmentation and center point estimation are obtained using our proposed training-free binary clustering algorithm. Finally, the robot executes the grasping operation based on the obtained position, with the results shown in Fig. 3.

In more detail, as shown in Fig. 3, scenes 1 and 2 are tested using the combination 1, while scenes 3 through 6 are tested using the combination 2. The first image in each column provides an enlarged view of the object placement within the scene. Specifically, scenes 1 and 5 involve scattered object placements, scenes 2 and 6 involve complex object stacking, and scenes 3 and 4 involve densely packed objects. The experimental results show that our proposed pipeline performs excellent in recognizing and grasping objects across all six scenes. In scene 4, although all objects are successfully identified, the robot fails to grasp the green bottle. Our

analysis indicates that the robot's gripper shape is not suitable for handling slender and smooth objects. The results from these six scenes demonstrate the excellent generalization and robustness of our algorithm across different devices and objects. Table II also presents the detailed numeric results for these six scenes. The symbol *R* represents the recognition rate, while *G* denotes the grasping rate, with values expressed as *success/total*.

TABLE II: Recognition rate (Recog.) and grasping rate (Grasp.) of our pipeline across various open-world scenarios with different device combinations. The performance of combination 1 is assessed in two scenarios, while combination 2 is tested in four scenarios.

	Scenario 1		Scenario 2	
	Recog.	Grasp.	Recog.	Grasp.
Combination 1	100%	100%	100%	100%
	Scenario 3	Scenario 4	Scenario 5	Scenario 6
	Recog.	Grasp.	Recog.	Grasp.
Combination 2	100%	100%	100%	88.9%
	100%	100%	100%	100%

V. FUTURE WORK

In this paper, we set up the camera above the robot in order to capture the entire scene. However, due to the precision limitations of point cloud acquisition devices, the potential error range in camera measurements can be quite large when the distance between the camera and the objects is significant, particularly for depth measurements. We have observed that the Intel RealSense D455 camera's point cloud modeling performance deteriorates significantly when the capture distance exceeds 1 meter, resulting in considerable depth discrepancies on the same horizontal plane. Therefore, in our future work, we plan to mount the camera on the robot to employ an eye-in-hand configuration for grasping. This approach will enable depth data modeling from multiple angles, helping the robot make timely and accurate assessments of the surrounding scene, and thereby improving grasping accuracy and reliability in open-world scenarios.

VI. CONCLUSION

We propose a cross-device pipeline that can grasp arbitrary objects in open-world scenarios without the need for training. Our pipeline delivers outstanding generalization and reliability across different hardware devices, effectively adapting to various real-world scenarios. The binary clustering algorithm we developed can be seamlessly integrated with any segmentation algorithm, enhancing both segmentation accuracy and pose estimation precision. In our experiments, the algorithm was deployed on multiple hardware platforms and tested in several open-world scenes. The results have demonstrated that our method can accurately grasp both seen and unseen objects in complex scenes, showcasing its strong generalization and robustness. In the future, we plan to explore an eye-in-hand hardware configuration to enhance the pipeline's performance in more challenging scenarios, further advancing the practical application of this task.

REFERENCES

[1] K. N. Kaipa, A. S. Kankanhalli-Nagendra, N. B. Kumbla, S. Shriyam, S. S. Thevendria-Karthic, J. A. Marvel, and S. K. Gupta, “Addressing perception uncertainty induced failure modes in robotic bin-picking,” *RCIM*, vol. 42, pp. 17–38, 2016.

[2] S. D’Avella, C. A. Avizzano, and P. Tripicchio, “Ros-industrial based robotic cell for industry 4.0: Eye-in-hand stereo camera and visual servoing for flexible, fast, and accurate picking and hooking in the production line,” *RCIM*, vol. 80, p. 102453, 2023.

[3] A. Amorim, D. Guimares, T. Mendona, P. Neto, P. Costa, and A. P. Moreira, “Robust human position estimation in cooperative robotic cells,” *RCIM*, vol. 67, p. 102035, 2021.

[4] Y. Jiang, Z. Huang, B. Yang, and W. Yang, “A review of robotic assembly strategies for the full operation procedure: planning, execution and evaluation,” *RCIM*, vol. 78, p. 102366, 2022.

[5] Y. Domae, H. Okuda, Y. Taguchi, K. Sumi, and T. Hirai, “Fast graspability evaluation on single depth maps for bin picking with general grippers,” in *ICRA*, pp. 1997–2004, 2014.

[6] R. Matsumura, K. Harada, Y. Domae, and W. Wan, “Learning based industrial bin-picking trained with approximate physics simulator,” in *IAS*, pp. 786–798, 2019.

[7] B. Drost, M. Ulrich, N. Navab, and S. Ilic, “Model globally, match locally: Efficient and robust 3d object recognition,” in *CVPR*, pp. 998–1005, Ieee, 2010.

[8] S. Hinterstoisser, V. Lepetit, S. Ilic, S. Holzer, G. Bradski, K. Konolige, and N. Navab, “Model based training, detection and pose estimation of texture-less 3d objects in heavily cluttered scenes,” in *ACCV*, pp. 548–562, Springer, 2013.

[9] B. Tekin, S. N. Sinha, and P. Fua, “Real-time seamless single shot 6d object pose prediction,” in *CVPR*, pp. 292–301, 2018.

[10] S. H. Bengtson, H. Åström, T. B. Moeslund, E. A. Topp, and V. Krueger, “Pose estimation from rgb images of highly symmetric objects using a novel multi-pose loss and differential rendering,” in *IROS*, pp. 4618–4624, 2021.

[11] T. Hodan, D. Barath, and J. Matas, “Epos: Estimating 6d pose of objects with symmetries,” in *CVPR*, pp. 11703–11712, 2020.

[12] C. Wang, D. Xu, Y. Zhu, R. Martín-Martín, C. Lu, L. Fei-Fei, and S. Savarese, “Densefusion: 6d object pose estimation by iterative dense fusion,” in *CVPR*, pp. 3343–3352, 2019.

[13] Y. He, H. Huang, H. Fan, Q. Chen, and J. Sun, “Ffb6d: A full flow bidirectional fusion network for 6d pose estimation,” in *CVPR*, pp. 3003–3013, 2021.

[14] Y. Di, R. Zhang, Z. Lou, F. Manhardt, X. Ji, N. Navab, and F. Tombari, “Gpv-pose: Category-level object pose estimation via geometry-guided point-wise voting,” in *CVPR*, pp. 6781–6791, 2022.

[15] F. Duffhauss, S. Koch, H. Ziesche, N. A. Vien, and G. Neumann, “Symfm6d: Symmetry-aware multi-directional fusion for multi-view 6d object pose estimation,” *RA-L*, 2023.

[16] H.-S. Fang, C. Wang, M. Gou, and C. Lu, “Grasnet-1billion: A large-scale benchmark for general object grasping,” in *CVPR*, pp. 11444–11453, 2020.

[17] J. Mahler, M. Matl, V. Satish, M. Danielczuk, B. DeRose, S. McKinley, and K. Goldberg, “Dex-net 2.0: Deep learning to plan robust grasps with synthetic point clouds and analytic grasp metrics,” in *ICRA*, pp. 291–298, 2017.

[18] D. Kalashnikov, A. Irpan, P. Pastor, J. Ibarz, A. Herzog, E. Jang, D. Quillen, E. Holly, M. Kalakrishnan, V. Vanhoucke, et al., “Scalable deep reinforcement learning for vision-based robotic manipulation,” in *CoRL*, pp. 651–673, 2018.

[19] W. Zhao, Y. Yan, C. Yang, J. Ye, X. Yang, and K. Huang, “Divide and conquer: 3d point cloud instance segmentation with point-wise binarization,” in *ICCV*, pp. 562–571, 2023.

[20] T. Vu, K. Kim, T. M. Luu, T. Nguyen, and C. D. Yoo, “Softgroup for 3d instance segmentation on point clouds,” in *CVPR*, pp. 2708–2717, 2022.

[21] L. Jiang, H. Zhao, S. Shi, S. Liu, C.-W. Fu, and J. Jia, “Pointgroup: Dual-set point grouping for 3d instance segmentation,” in *CVPR*, pp. 4867–4876, 2020.

[22] A. Dai, M. Nießner, M. Zollhöfer, S. Izadi, and C. Theobalt, “Bundle-fusion: Real-time globally consistent 3d reconstruction using on-the-fly surface reintegration,” *ACM Transactions on Graphics (ToG)*, vol. 36, no. 4, p. 1, 2017.

[23] Y. Guo, H. Wang, Q. Hu, H. Liu, L. Liu, and M. Bennamoun, “Deep learning for 3d point clouds: A survey,” *TPAMI*, vol. 43, no. 12, pp. 4338–4364, 2020.

[24] J. Bohg, A. Morales, T. Asfour, and D. Kragic, “Data-driven grasp synthesis - A survey,” *T-RO*, vol. 30, no. 2, pp. 289–309, 2014.

[25] J. Tobin, L. Biewald, R. Duan, M. Andrychowicz, A. Handa, V. Kumar, B. McGrew, A. Ray, J. Schneider, P. Welinder, et al., “Domain randomization and generative models for robotic grasping,” in *IROS*, pp. 3482–3489, 2018.

[26] J. Tobin, R. Fong, A. Ray, J. Schneider, W. Zaremba, and P. Abbeel, “Domain randomization for transferring deep neural networks from simulation to the real world,” in *IROS*, pp. 23–30, 2017.

[27] X. B. Peng, M. Andrychowicz, W. Zaremba, and P. Abbeel, “Sim-to-real transfer of robotic control with dynamics randomization,” in *ICRA*, pp. 3803–3810, IEEE, 2018.

[28] A. Bicchi and V. Kumar, “Robotic grasping and contact: A review,” in *ICRA*, pp. 348–353, 2000.

[29] L. Yu, Y. Jin, L. Qiao, G. Jin, S. Qin, and Y. Chen, “A variable stiffness gripper with dual leaf-spring mechanism,” in *CASE*, pp. 1–7, 2023.

[30] S. Ainetter and F. Fraundorfer, “End-to-end trainable deep neural network for robotic grasp detection and semantic segmentation from RGB,” in *ICRA*, pp. 13452–13458, 2021.

[31] I. Lenz, H. Lee, and A. Saxena, “Deep learning for detecting robotic grasps,” *IJRR*, vol. 34, no. 4-5, pp. 705–724, 2015.

[32] Y. Yan, L. Tong, K. Song, H. Tian, Y. Man, and W. Yang, “Sisgnet: Simultaneous instance segmentation and grasp detection for robot grasp in clutter,” *ADVEI*, vol. 58, p. 102189, 2023.

[33] F.-J. Chu, R. Xu, and P. A. Vela, “Real-world multiobject, multigrasp detection,” *RA-L*, vol. 3, no. 4, pp. 3355–3362, 2018.

[34] J. Mahler, M. Matl, V. Satish, M. Danielczuk, B. DeRose, S. McKinley, and K. Goldberg, “Learning ambidextrous robot grasping policies,” *Science Robotics*, vol. 4, no. 26, p. 4984, 2019.

[35] G. Tzifas and H. Kasaei, “Towards open-world grasping with large vision-language models,” *arXiv preprint arXiv:2406.18722*, 2024.

[36] J. Huang, S. Yong, X. Ma, X. Linghu, P. Li, Y. Wang, Q. Li, S.-C. Zhu, B. Jia, and S. Huang, “An embodied generalist agent in 3d world,” in *ICML*, 2024.

[37] S. Jin, J. Xu, Y. Lei, and L. Zhang, “Reasoning grasping via multi-modal large language model,” *arXiv preprint arXiv:2402.06798*, 2024.

[38] Y. Hong, Z. Zheng, P. Chen, Y. Wang, J. Li, and C. Gan, “Multiply: A multisensory object-centric embodied large language model in 3d world,” in *CVPR*, pp. 26406–26416, 2024.

[39] S. Dong, G. Lin, and T.-Y. Hung, “Learning regional purity for instance segmentation on 3d point clouds,” in *ECCV*, pp. 56–72, 2022.

[40] A. Chen, K. Zhang, R. Zhang, Z. Wang, Y. Lu, Y. Guo, and S. Zhang, “Pimae: Point cloud and image interactive masked autoencoders for 3d object detection,” in *CVPR*, 2023.

[41] T. He, C. Shen, and A. van den Hengel, “Dyco3d: Robust instance segmentation of 3d point clouds through dynamic convolution,” in *CVPR*, pp. 354–363, 2021.

[42] Y. Wu, M. Shi, S. Du, H. Lu, Z. Cao, and W. Zhong, “3d instances as 1d kernels,” in *ECCV*, pp. 235–252, 2022.

[43] B. Li, W. Ouyang, L. Sheng, X. Zeng, and X. Wang, “Gs3d: An efficient 3d object detection framework for autonomous driving,” in *CVPR*, pp. 1019–1028, 2019.

[44] B. Graham, “Sparse 3d convolutional neural networks,” in *BMVC*, pp. 150–159, 2015.

[45] S. Chen, J. Fang, Q. Zhang, W. Liu, and X. Wang, “Hierarchical aggregation for 3d instance segmentation,” in *ICCV*, pp. 15467–15476, 2021.

[46] M. Zhong, X. Chen, X. Chen, G. Zeng, and Y. Wang, “Maskgroup: Hierarchical point grouping and masking for 3d instance segmentation,” in *ICME*, pp. 1–6, 2022.

[47] A. Dai, A. X. Chang, M. Savva, M. Halber, T. Funkhouser, and M. Nießner, “Scannet: Richly-annotated 3d reconstructions of indoor scenes,” in *CVPR*, 2017.

[48] Z. Liang, Z. Li, S. Xu, M. Tan, and K. Jia, “Instance segmentation in 3d scenes using semantic superpoint tree networks,” in *ICCV*, pp. 2783–2792, 2021.